Genome-wide RAD sequencing data suggest predominant role of vicariance in Sino-Japanese disjunction of the monotypic genus Conandron (Gesneriaceae)

Article *in* Journal of Systematics and Evolution · December 2022

DOI: 10.1111/jse.12937

6 authors, including:

Shao-Jun Ling
Hainan University
17 PUBLICATIONS **32** CITATIONS
SEE PROFILE

Jordi López-Pujol
Institut Botànic de Barcelona
253 PUBLICATIONS **2,522** CITATIONS
SEE PROFILE

Ke Tan
Hainan University
9 PUBLICATIONS **36** CITATIONS
SEE PROFILE

Ming-Xun Ren
Hainan University
74 PUBLICATIONS **681** CITATIONS
SEE PROFILE

JSE Journal of Systematics and Evolution

doi: 10.1111/jse.12937

Research Article

Genome-wide RAD sequencing data suggest predominant role of vicariance in Sino-Japanese disjunction of the monotypic genus *Conandron* (Gesneriaceae)

Shao-Jun Ling[1,2†], Xiao-Lan Yao[1,2†], Juli Caujapé-Castells[3], Jordi López-Pujol[4,5], Ke Tan[1,2*], and Ming-Xun Ren[1,2*]

[1]Ministry of Education Key Laboratory for Genetics and Germplasm Innovation of Tropical Special Forest Trees and Ornamental Plants, Hainan University, Haikou 570228, China

[2]Center for Terrestrial Biodiversity of South China Sea, Hainan University, Haikou 570228, China

[3]The Jardín Botánico Canario "Viera y Clavijo"—UA CSIC (Cabildo de Gran Canaria), 35017 Las Palmas de Gran Canaria, Spain

[4]Botanic Institute of Barcelona (IBB), CSIC—Ajuntament de Barcelona, Barcelona 08038, Spain

[5]Escuela de Ciencias Ambientales, Universidad Espíritu Santo (UEES), Samborondón 091650, Ecuador

[†]These authors contributed equally to this study.

*Authors for correspondence. Ke Tan. E-mail: tanke@hainanu.edu.cn; Ming-Xun Ren. E-mail: renmx@hainanu.edu.cn

Received 13 September 2022; Accepted 24 November 2022; Article first published online 16 December 2022

Abstract Disjunct distribution is a key issue in biogeography and ecology, but it is often difficult to determine the relative roles of dispersal vs. vicariance in disjunctions. We studied the phylogeographic pattern of the monotypic *Conandron ramondioides* (Gesneriaceae), which shows Sino-Japanese disjunctions, with ddRAD sequencing based on a comprehensive sampling of 11 populations from mainland China, Taiwan Island, and Japan. We found a very high degree of genetic differentiation among these three regions, with very limited gene flow and a clear Isolation by Distance pattern. Mainland China and Japan clades diverged first from a widespread ancestral population in the middle Miocene, followed by a later divergence between mainland China and Taiwan Island clades in the early Pliocene. Three current groups have survived in various glacial refugia during the Last Glacial Maximum, and experienced contraction and/or bottlenecks since their divergence during Quaternary glacial cycles, with strong niche divergence between mainland China + Japan and Taiwan Island ranges. Thus, we verified a predominant role of vicariance in the current disjunction of the monotypic genus *Conandron*. The sharp phylogenetic separation, ecological niche divergence among these three groups, and the great number of private alleles in all populations sampled indicated a considerable time of independent evolution, and suggests the need for a taxonomic survey to detect potentially overlooked taxa.

Key words: demography, ecological niche differences, isolation by distance, phylogeography, relict plant, species distribution model.

1 Introduction

Due to its vast extension, stretching from boreal to tropical ecosystems, East Asia is a key region for relict species/lineages that survived the Cenozoic climatic deterioration, and thus often presents complicated species distribution patterns, for example, disjunctions (Qiu et al., 2009, 2011; Qi et al., 2014; Tang et al., 2018). Traditionally, two alternative explanations have been proposed to explain species disjunct distributions (Tallis, 1991), that is long-distance dispersal across pre-existing geographical barriers, or the fragmentation of a widespread ancestral range (vicariance) by the formation of geographical barriers such as mountain uplifts and marine transgressions. The role of dispersal vs. vicariance has for decades fascinated scientists in the fields of biogeography and evolutionary ecology, but the relative contribution of these diversification forces to current species geographic patterns is still debated, partly due to the elusiveness of extinction and the high numbers of biotic, abiotic and stochastic factors that overlap throughout the geological ontogeny of each region (Caujapé-Castells et al., 2017).

Conandron ramondioides Siebold & Zucc. is the only species of the genus *Conandron* Siebold & Zucc. (Gesneriaceae), with a disjunct distribution in mainland China (in four provinces: Anhui, Fujian, Jiangxi, and Zhejiang), Taiwan Island, and the Japanese islands (Honshu, Kyushu, Shikoku, and the Ryukyus) (Wang, 2004; Wang et al., 2010; Xiao et al., 2012). This monotypic genus is distinctive for its radially symmetrical corolla with four fertile stamens and cohesive anthers (Wang et al., 2010). The molecular data available indicate that *C. ramondioides* is a relict taxon that probably

split from its closest relatives ca. 30 Ma (Roalson & Roberts, 2016), making it phylogenetically distinct from other taxa in the Old World Gesneriaceae (Wang, 2004; Weber, 2004; Wang et al., 2010; Roalson & Roberts, 2016). Although several studies have explored the population differentiation of its Chinese populations with DNA markers (Xiao, 2005; Xiao et al., 2012), a detailed study sampling the whole range (including mainland China, Taiwan Island, and Japan) using updated molecular methods is still needed to explore the processes underlying its phylogenetically isolated condition within the Gesneriaceae and the evolutionary history of plant disjunctions in this species-rich region.

Here, we use restriction site-associated DNA sequencing (RAD-seq) on extensive sampling of *C. ramondioides* in mainland China, Taiwan Island, and Japanese islands, to investigate its phylogeographic structure and (putative) genetic barriers, population divergence models, and demographic scenarios, and to evaluate the effects of past climate changes on distribution ranges and test for ecological niche differentiation, with a final note about the role of dispersal vs. vicariance in the shaping of current East Asia flora.

2 Material and Methods

2.1 Sampling and DNA extraction

Conandron ramondioides is a perennial and rhizomatous herb that usually grows on wet and moss-covered granite rocks in mountain cliffs and valleys (Wang, 2004; Xiao et al., 2012). Its local populations are usually highly fragmented and restricted to isolated mountain areas (Wang, 2004; Xiao, 2005). We sampled a total of 11 populations of *C. ramondioides* covering its whole distribution range as described in the *Flora of China* (Wang et al., 1998) and *Flora of Japan* (Yamazaki, 1993) (Table 1). All samples were dried and stored in the field in silica gel. Voucher specimens were deposited in the Herbarium of Hainan University (HUTB; Table 1). In total, 108 individuals of *C. ramondioides* were sampled and studied, with three individuals of *Ridleyandra* A. Weber & B.L. Burtt (phylogenetically close to *Conandron*; Roalson & Roberts, 2016) used as outgroup. The total genomic DNA was extracted from young leaves using a modified cetrimonium bromide (CTAB) protocol adapted from Doyle & Doyle (1987). The DNA quality was assessed using a 1.0% agarose gel.

2.2 RAD library preparation and sequencing

In total, 100 ng genomic DNA from each individual were digested using two restriction enzymes, *Eco*RI and *Pst*I (New England Biolabs, Beverly, USA), at 37 °C for 8 h. The restriction enzymes were then inactivated by heating at 65 °C for 20 min. After ligation with individually barcoded *Eco*RI adapter and universal *Pst*I adapter with T4 DNA ligase for each sample at 16 °C for 8 h, the reaction was stopped by heating at 65 °C for 20 min. The ligation products of 24 samples were pooled equally and size selected into 300–500-bp fragments using agarose gel electrophoresis. After the gel purification step, the derived fragments were used as templates (ca. 30 ng) for PCR amplification via 25 cycles with *Eco*RI and *Pst*I adapter universal primers and PrimeStar Max DNA polymerase (TaKaRa, Dalian, China). Finally, the amplicons were size selected once more into 350–500-bp fragments using the method mentioned previously. The resulting ddRAD library was sent to the Guangzhou Jierui Biotechnology Company (Guangzhou, China) and sequenced on an Illumina NovaSeq platform using the 150 nt with paired-end mode.

2.3 De novo clustering and single nuclear polymorphism (SNP) exploitation

We used the *process_radtags* module in the Stacks v.2.4 program (Catchen et al., 2013) to de-multiplex the raw data, setting all parameters as default. We also trimmed all the reads to 135 bp in length to remove low-quality nucleotides at the 3′ end of each read. Each end of the retained reads was treated as an independent locus, and we combined all of them for the statistical analyses. We first used the *ustacks* module in Stacks to cluster the reads into exactly matching stacks. Here we set $m = 2$ as the minimum depth of coverage (m) and $M = 12$ as the maximum distance allowed between stacks within an individual. We then used the *cstacks* module to build the catalogs for all 111 individuals with $n = 12$ as the maximum number of mismatches allowed between individuals. The *sstacks* module was used to generate alignment results for each individual against the catalog using default parameters. In the population module, we set $P = 10$ and

Table 1 Collection location, site ID and geographical coordinates of sampled populations of *Conandron ramondioides*

Code	Location	*N*	Latitude/longitude	Elevation (m)	Voucher
JP-YD	Izu Peninsula, Shizuoka Pref., Japan	7	34°41′05″N/138°53′52″E	100	Ren2018061601
JP-CB	Kiyosumi, Chiba Pref., Japan	8	35°08′37″N/140°08′19″E	90	Ren2018070201
JP-CCB	Ochigawa, Chichibu, Saitama Pref., Japan	8	36°02′41″N/138°57′13″E	545	Ren2018072801
MC-HS	Huangshan, Anhui Prov., China	16	30°07′21″N/118°10′31″E	1158	…
MC-WY	Tuochuan, Wuyuan, Jiangxi Prov., China	5	29°32′47″N/117°46′54″E	821	Hou2020060301
MC-YX	Youxi, Fujian Prov., China	7	26°08′25″N/118°32′31″E	657	…
MC-HZ	Damingshan, Hangzhou, Zhejiang Prov., China	13	30°02′16″N /118°59′13″E	556	…
MC-TZ	Kuocangshan, Taizhou, Zhejiang Prov., China	8	28°32′40″N/120°35′36″E	710	Hou2020052501
MC-TS	Wuyanling, Taishun, Zhejiang Prov., China	10	27°21′04″N /119°56′13″E	539	…
TW-XZ	Yuanyang Valley, Xinzhu, Taiwan Prov., China	11	24°34′54″N/121°17′22″E	973	Ren2019061601
TW-NT	Xitou Nature Park, Nantou, Taiwan Prov., China	15	23°55′11″N /120°40′12″E	1379	Ren2019062401

N, number of sampled individuals; Pref., prefecture (the first-level administrative division in Japan); Prov., province (the first-level administrative division in China).

$r = 0.6$ to call the consensus SNPs among 108 individuals, which requires SNPs to be found in at least eight populations and 60% of individuals within one population. The *phylip*, *structure*, and *vcf* files were generated and the data were filtered using VCFtools (Danecek et al., 2011) for subsequent analysis. PGDspider v.2.02 (Lischer & Excoffier, 2012) was used subsequently for file conversion to program-specific formats.

2.4 Population genetic structure

Genetic summary statistics for ddRAD-seq genomic data, including the percentage of polymorphic sites (%*P*), observed and expected heterozygosity (H_O and H_E), nucleotide diversity (π), and inbreeding coefficient (F_{IS}), were estimated using *populations* in Stacks for all populations (11) with more than five samples. Pairwise F_{ST} values were calculated using Arlequin v.3.5.2.2 (Excoffier & Lischer, 2010), with 10 000 permutations. In order to test the degree of population divergence relevant to gene flow, *Nm* among populations was calculated according to Wright (1951). Hierarchical analysis of molecular variance (AMOVA) was implemented based on our assessment of the hierarchical population structure ($K = 2$ and 3; see Sections 3 and 4) in order to quantify genetic variation partitioning across the different sampling levels.

To evaluate admixture in all populations of *C. ramondioides*, we used the maximum-likelihood (ML) method implemented in ADMIXTURE v.1.3.0 to estimate individual admixture (Alexander et al., 2009; Decker et al., 2014). This method allowed for uncertainty in ancestral allele frequencies. We predefined the number of populations as $K = 1$–12. Ten independent runs were performed for each value of *K*. The optimal *K* was chosen using the lowest cross-validation (CV) error.

We further performed a principal components analysis (PCA) to visualize the major axes of genetic variation using the *Adegenet* package (*glPCA* function; Jombart, 2008) in R. Then we used *ggplot2* to plot the PCA, color the samples by population, and create ellipses that included 95% of the data for each population.

2.5 Phylogeny and genetic differentiation

We estimated an ML phylogeny of the 11 populations from unlinked SNPs with a GTR substitution matrix and GAMMA model using RAxML v.8.2.6 (Stamatakis, 2006). Three individuals of *Ridleyandra* were used as outgroups. Nodal support was estimated using 1000 bootstrap replicates.

To investigate the correlation between genetic and geographic distances, we used GenAlEx v.6.5 to perform a Mantel test at the population level. The genetic distance matrix was obtained from the pairwise F_{ST} values calculated in Arlequin v.3.5.2.2 (Excoffier & Lischer, 2010), and the geographic distance matrix (i.e., the straight-line distances between each possible population pair) was generated from the latitude and longitude coordinates.

In order to determine the occurrence of gene exchange barriers along the species range, we used BARRIER v.2.2 (Manni et al., 2004) to identify the areas of maximum variation between populations according to Monmonier's (1973) maximum-difference algorithm. The genetic distance matrix (F_{ST}) between two populations and the latitude and longitude data of each population were imported into the software, and the number of barriers was set to 3.

2.6 Estimates of historical demography

We used DIYABC v.2.1.0 software to explore the historical demography of *C. ramondioides*, which uses an approximate Bayesian computation (ABC) algorithm (Cornuet et al., 2014). Based on the results of ADMIXTURE, PCA, and phylogenetic tree of *C. ramondiodes*, the 11 studied populations were classified into three groups, that is Group MC (mainland China), Group TW (Taiwan Island), and Group JP (Japan). The JP clade was located at the base of the phylogenetic tree, thus we first tested six possible divergence scenarios to estimate whether *C. ramondiodes* originated from Japanese islands (Fig. S1A). We selected a single SNP per locus, which had to be present in at least 70% of the individuals in all three groups. The simulated SNP data set was obtained using the algorithm proposed by Hudson (2002). A uniform prior probability was used, and all summary statistics were selected to generate a reference table, based on 6×10^6 simulated data sets. To estimate the relative posterior probabilities for each scenario, we used the 1% simulated data sets closest to the observed data to obtain a logistic and posterior distribution of historical demographic parameters according to the most likely scenario (Cornuet et al., 2010). A conservative estimate for generation time to 3 years to estimate the demographic history of *C. ramondiodes* was set based on our field observations. In order to choose the best fit demographic scenario and parameter estimation, surveys in the three groups of *C. ramondiodes* were carried out using four models of changes in population size with the same parameter settings (Fig. S1B).

2.7 Species distribution models

Species distribution models for *C. ramondioides* for the Last Interglacial period (LIG; ca. 120 000 years before present [BP]), Last Glacial Maximum (LGM; ca. 21 000 years BP), and current and future (year 2070) periods, were generated using MaxEnt v.3.4.1 (https://biodiversityinformatics.amnh.org/open_source/maxent/; Phillips et al., 2006). In addition to our sampling sites, the distribution records for *C. ramondioides* sourced from the Global Biodiversity Information Facility (GBIF; http://www.gbif.org), the Chinese Virtual Herbarium (http://www.cvh.org.cn), and the National Specimen Information Infrastructure (NSII; http://www.nsii.org.cn/) were also included; in total, 74 *C. ramondioides* occurrence sites were acquired to build the models (Table S1). Duplicate records within $30'' \times 30''$ cells were removed to reduce the effects of spatial autocorrelation under different climate variations. The bioclimatic layers for the LIG (Otto-Bliesner et al., 2006), current and future (Community Climate System Model Version 4 [CCSM4]; Gent et al., 2011) climate data were retrieved from the WorldClim 1.4 website (http://www.worldclim.org; Hijmans et al., 2005) at $30''$ spatial resolution (ca. 1 km^2 on the ground). The year 2070 model was run under RCP 8.5, which represents the highest emission scenario (an increase of 2.6–4.8 °C; Collins et al., 2013). For the LGM, we took data from three climatic models offered by the WorldClim website, CCSM4, the Model for Interdisciplinary Research on Climate (MIROC; Watanabe

et al., 2011) and the New Earth System Model of the Max Planck Institute for Meteorology (MPI-ESM-P: http://www.mpimet.mpg.de/en/science/models/mpi-esm/), at a scale of 2.5′ × 2.5′ (which were later resampled to 30″ resolution). Nine uncorrelated and biologically significant bioclimatic variables were selected as predictors, after Pearson correlation coefficients analysis with $|r|<0.8$ of each pairwise comparison of 19 bioclimatic variables in SPSS v.20.0. Model validation was carried out using default settings with 10 bootstrap replicates and 10 000 background points of CV procedures with 25% of the point data used for model testing. The contribution of each variable was assessed using the jackknife approach (Baldwin, 2009), and the performance of each model was evaluated by the area under the receiver operating characteristic curve (AUC; Fielding & Bell, 1997; Wang et al., 2007), with value >0.9 indicating good prediction (Swets, 1988). The MaxEnt results were categorized into a highly suitable area (0.75–1.00), moderately suitable area (0.50–0.75), low suitable area (0.25–0.50), and unsuitable area (0–0.25) based on logistic probability values.

2.8 Niche comparisons in environmental space

To test if the currently realized niches (environmental space) of the three identified clades of *C. ramondioides* (mainland China, Taiwan Island, and Japan) differed significantly from each other or shared common climatic characteristics (i.e., niches have either diverged or are conserved), we used the principal component analysis of environmental variables (PCA-env) comparison framework (Broennimann et al., 2012; Silva et al., 2016; Herrando-Moraira et al., 2019) using the R Core platform (2021). The same occurrences and uncorrelated and biologically significant bioclimatic variables for species distribution modeling (SDM) were inputted. The original occurrences were trimmed to guarantee a minimum distance of 5 km between them using the "thin" function of the *spThin* R package (Aiello-Lammens et al., 2015), followed by a correction with a kernel smoother density function (Broennimann et al., 2012, 2014). Finally, in total, 74 input occurrences were obtained. Then we projected the smoothed densities into a global environmental space with a 100 × 100 grid-cell resolution, making each cell a sole combination of climatic conditions. The global environmental space was delimited with the background areas, based on a minimum convex polygon with a buffer size of 0.3° as Silva et al. (2016). The PCA-env plots were visualized as the individual plots for each of the three geographic regions and the global plot in which all tested niches were simultaneously represented.

The levels of niche divergence/conservatism were quantified between pairs of the defined geographic units, that is mainland China, Taiwan Island, and Japan, using Schoener's D_S niche overlap metric (Schoener, 1970; Warren et al., 2008), which ranges from 0 (no overlap scenario) to 1 (completely overlap scenario).

To assess whether compared niches were more equivalent or similar than expected by chance, the niche equivalency and niche similarity tests were computed (Broennimann et al., 2012). The main difference between the two tests was that the former only considered the occurrences, while the latter also took into account the surrounding areas where the predefined units occur. In the two tests, the observed D_S values (D_{obs}) were compared with a null distribution of 100 simulated D_S values (D_{sim}), with three possible scenarios after a two-tailed test: (1) $D_{obs} > D_{sim}$ with $P < 0.05$, indicating that niches are more equivalent or similar than randomly expected; (2) $D_{obs} < D_{sim}$ with $P < 0.05$, indicating that niches are less equivalent or similar than expected by chance; (3) if D_{obs} falls within 95% of D_{sim} values with $P > 0.05$, the null hypothesis of niche equivalency or similarity cannot be rejected.

To infer niche conservatism (more equivalency or similarity) or niche divergence (less equivalency or similarity), both analyses were run twice in a one-tailed test with the argument "alternative" set to "lower" or "higher" in the function "ecospat.niche.similarity.test" and "ecospat.niche.equivalency.test" (R package "ecospat"; Broennimann et al., 2014).

3 Results

3.1 Sequence data quality and genetic diversity

In total, 108 individuals of *Conandron ramondioides* were sequenced using seven lanes of Illumina that produced in total >425 million reads. Over 7 million reads passed our quality control and over 418 million reads in total were used in the assembly of the RAD-tags. After SNP filtering, we obtained 2194 RAD loci containing 16 206 SNPs that could be used for population genetic analyses.

Based on 19 668 polymorphic sites, the average percentage of genomic polymorphic sites (%*P*) for each population was 0.968 and ranged from 0.957 to 0.976 (Table 2). Private alleles were present in all populations and varied from 279 (MC-HS population) to a maximum of 1302 (JP-CB population). Observed heterozygosity (H_O) across populations ranged from 0.029 to 0.057 for each population (average = 0.040), and expected heterozygosity (H_E) ranged from 0.042 to 0.062 (average = 0.050). Expected heterozygosity was consistently higher than observed heterozygosity in all populations, and nucleotide diversity (π) across populations ranged from 0.030 to 0.061 (average =

Table 2 Genetic diversity statistics within the 11 sampled populations of *Conandron ramondioides*

Pop. code	PA	%*P*	H_E	H_O	π	F_{IS}
MC-HS	279	0.976	0.042	0.029	0.030	−0.021
MC-YX	497	0.973	0.045	0.033	0.036	−0.016
MC-WY	286	0.973	0.049	0.031	0.036	−0.024
MC-HZ	485	0.974	0.043	0.032	0.033	−0.017
MC-TZ	623	0.970	0.050	0.038	0.042	−0.014
MC-TS	640	0.966	0.055	0.042	0.045	−0.017
JP-YD	650	0.963	0.059	0.047	0.052	−0.011
JP-CB	1302	0.966	0.054	0.043	0.047	−0.011
JP-CCB	862	0.957	0.062	0.057	0.061	0.005
TW-XZ	1080	0.965	0.051	0.048	0.051	0.005
TW-NT	882	0.969	0.046	0.040	0.042	−0.001
Average	688.73	0.968	0.050	0.040	0.043	−0.011

F_{IS}, inbreeding coefficient; H_E, expected heterozygosity; H_O, observed heterozygosity; %*P*, percentage of polymorphic sites; PA, number of private alleles; π, nucleotide diversity.

0.043; Table 2).

Based on π and H_E values, within-population genomic diversity levels were generally rank-ordered per biogeographical area as JP > TW > MC (Table 2). The inbreeding coefficient (F_{IS}) ranged from −0.024 to 0.005, indicating no inbreeding within populations.

3.2 Population genetic structure

Pairwise F_{ST} values among populations ranged from 0.136 to 0.561 (average = 0.335), indicating high interpopulation differentiation. In particular, the large geographic distances between populations of mainland China and Taiwan Island + Japan corresponded to relatively high pairwise F_{ST} values (above 0.400, except for the pair TW-XZ/MC-TS with F_{ST} = 0.396), suggesting high levels of population differentiation between these regions. By contrast, the F_{ST} values between intra-mainland China populations were mostly between 0.250 and 0.350 (except F_{ST} = 0.169 between MC-WY and MC-HS) (Table S2). The gene flow among populations showed values that were less than 1, except for the pair MC-HS/MC-WY with Nm = 1.2322 and TW-NT/TW-XZ with Nm = 1.5916. In addition, the gene flow among regions showed values that were less than 0.47 (Table S3).

The ADMIXTURE software determined that the number of groups that maximized the clustering of genetically similar individuals together with the lowest CV error was K = 2 (Figs. 1A, 1B), although K = 3 was another reasonable clustering model. When K = 2, the 108 individuals were divided into those belonging to mainland China plus Taiwan Island populations (as one class) and Japanese populations (as another class). When K = 3, Taiwan Island populations were separated from those from mainland China.

Consistent with the K = 3 clustering in ADMIXTURE, the AMOVA showed a higher level of genetic differentiation among the three groups (Japan, mainland China, and Taiwan Island, variation = 45.91%) than among two groups (Japan vs. mainland China + Taiwan Island, variation = 24.12%); indeed, for K = 2 most variation was due to the among-populations within-groups component (61.71%) (Table 3). The PCA (Fig. 1C) also revealed three distinct clusters. Similarly, the ML phylogenetic analysis grouped the 108 individuals into three robust clades (>90% bootstrap support; Figs. 2B, S2).

The Mantel test showed a significant positive correlation between pairwise genetic distance and geographic distance (r = 0.499, P < 0.01; Fig. S3), and the BARRIER analysis indicated that there were three major genetic boundaries (isolation lines) among the studied populations (Fig. 2C): line "a" (which corresponds to Tokyo Bay, in Japan) separated JP-CB from the rest; line "b" (Taiwan Strait) separated the populations from Taiwan Island and mainland China; and line "c" (East China Sea) separated Chinese and Japanese populations.

3.3 Demographic history

DIYABC estimations of the divergence history of *C. ramondioides* indicated that Scenario 4 described the best fit to our data, with the highest posterior probability = 0.9997, 95% CI = 0.9582–1.0000 (Fig. 3A; Table S4), depicting the origin of both Group MC and Group JP from a common uncertain ancestor (Group MC + JP), and which would have split into the two lineages at ca. 11.850 Ma (95% CI: 6.810–15.660 Ma), followed by an origin of Group TW from Group MC at ca. 4.050 Ma (95% CI: 2.601–7.410 Ma). The best fit scenario of demographic history for both Group TW and Group JP was Scenario 2, and for Group MC was Scenario 3 (Fig. S1B). Group MC was found to experience a population

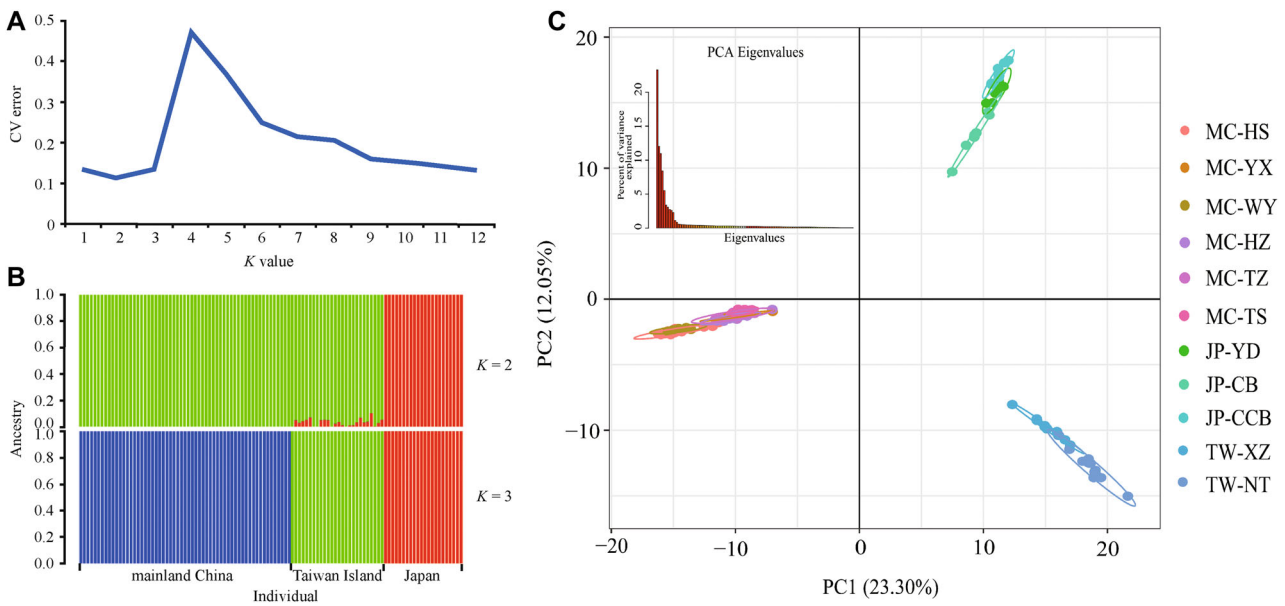

Fig. 1. Population genetic structure analysis based on single nuclear polymorphism (SNP) data of *Conandron ramondioides* individuals based on ADMIXTURE, with (**A**) values of cross-validation (CV) error at different K values and (**B**) clustering situations within all individuals of *C. ramondioides* when K = 2 and K = 3. **C**, Principal component analysis (PCA) based on SNP data of the 108 studied individuals of *C. ramondioides*, with the proportion of the variance explained being 23.30% for principal component (PC)1 and 12.05% for PC2. The insert figure plots the eigenvalues of different PCs.

Table 3 Analysis of molecular variance (AMOVA) based on SNP data of 108 *Conandron ramondioides* individuals

Scale	Source of variation	*df*	Sum of squares	Variance components	Percentage of variation
Total	Among populations	10	6232.524	74.69387	83.37
	Within populations	97	1183.551	14.89961	16.63
	Total	107	7416.075	89.59349	100.00
Define groups ($K = 2$)	Among groups	1	1292.298	25.36556	24.12
	Among populations within groups	9	4940.226	64.89554	61.71
	Within populations	97	1183.551	14.89961	14.17
	Total	107	7416.075	105.16071	100.00
Define groups ($K = 3$)	Among groups	2	3415.62	48.70373	45.91
	Among populations within groups	8	2816.904	42.47085	40.04
	Within populations	97	1183.551	14.89961	14.05
	Total	107	7416.075	106.07419	100.00

df, degrees of freedom.

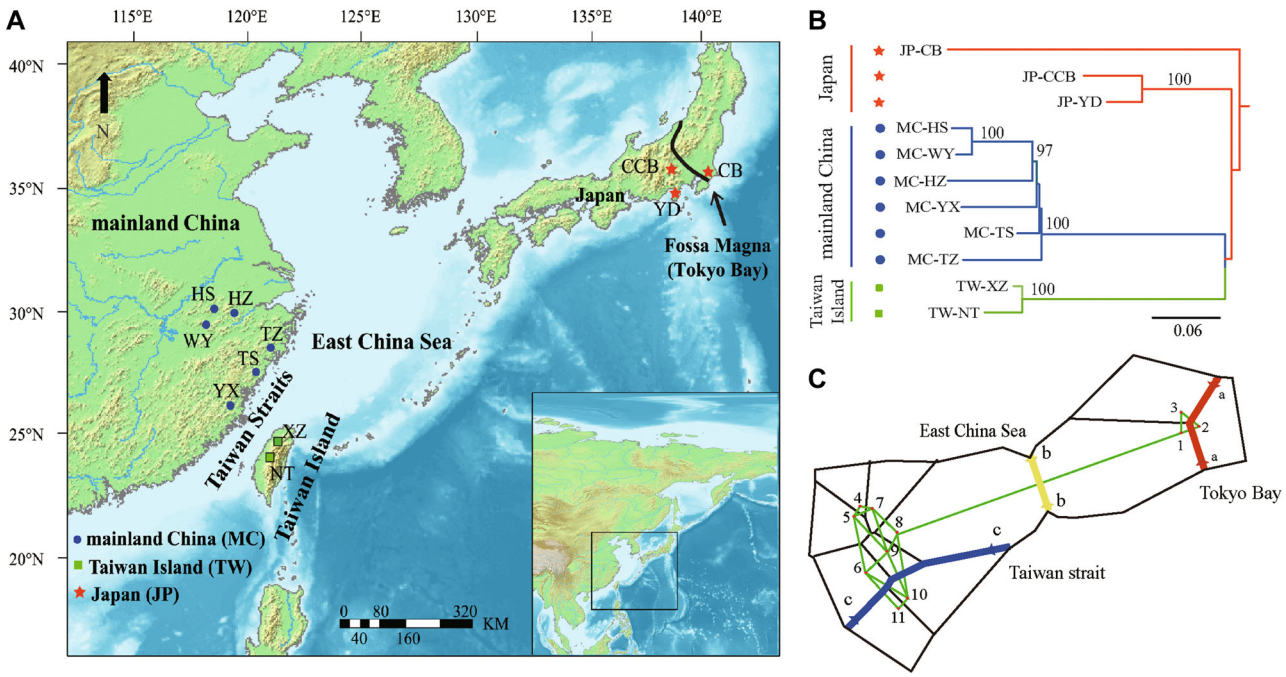

Fig. 2. A, Map of East Asia showing the studied *Conandron ramondioides* populations with (**B**) the maximum-likelihood phylogenetic tree using the RAD tag single nuclear polymorphisms (SNPs). Node support in the tree is given as the maximum parsimony bootstrap value, bootstrap values below 80% are not indicated. Colored bars and branches identify the three major genetic lineages. **C**, Major genetic boundaries detected among *C. ramondioides* populations using BARRIER v.2.2.

contraction at ca. 1.755 Ma (95% CI: 0.690–2.613 Ma). Group TW experienced a contraction at ca. 1.653 Ma (95% CI: 0.453–2.934 Ma), followed by expansion at ca. 0.166 Ma (95% CI: 0.049–0.289 Ma), whereas the contraction and expansion of Group JP would have taken place at ca. 0.804 Ma (95% CI: 0.471–1.116 Ma) and ca. 0.193 Ma (95% CI: 0.036–0.289 Ma), respectively (Figs. 3B, S1C).

3.4 Species distribution models

The AUC value was very high (mean ± SD = 0.971 ± 0.009; Fig. S4), indicating a high predictive power by MaxEnt. The most contributing bioclimatic variables in the four time periods considered were bio19 (precipitation in the coldest quarter), bio12 (annual precipitation), and bio10 (mean temperature of the warmest quarter) (Fig. S5; Table 4). The potentially suitable areas along the different climate scenarios showed relatively large changes (Table 5); detecting both range expansions and contractions between time periods (Table 6). The predictions for the LGM based on CCSM4, MIROC, and MPI-ESM-P were mostly consistent regarding total potential areas (i.e., a general range gain pattern compared with the present time; Table 5), except for moderately suitable areas that were much fewer in mainland China for the CCSM4 (Fig. 4). The model showed that some area loss (ca. 20%) is expected for the year 2070 under a

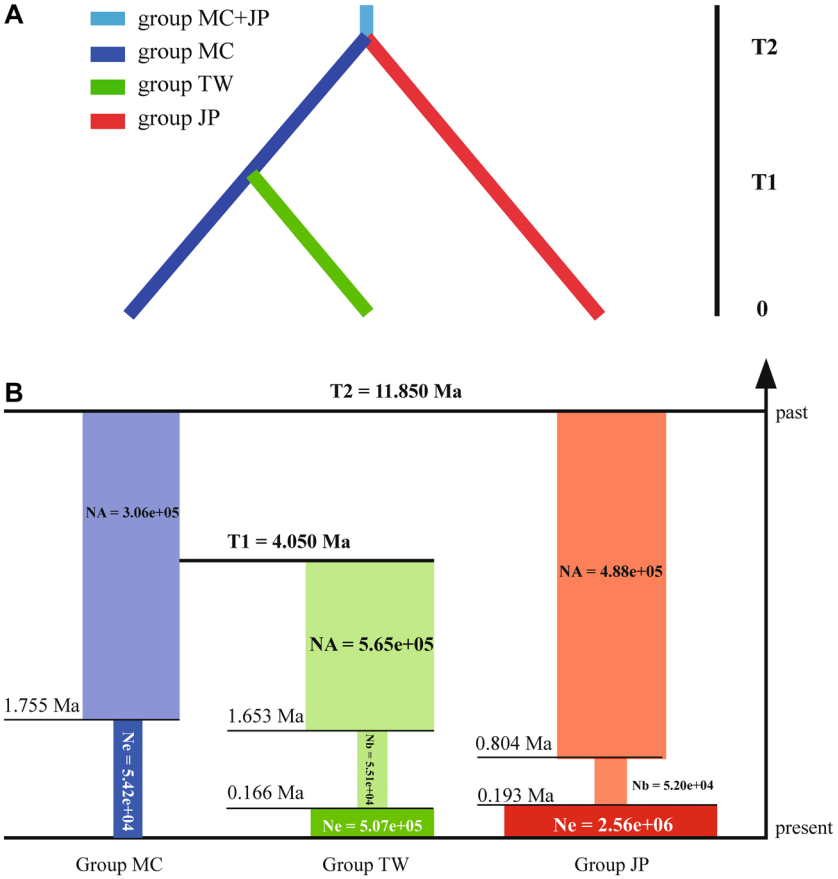

Fig. 3. A, The best approximate Bayesian computation (ABC) model for *Conandron ramondioides* based on DIYABC analysis. **B**, Demographic history of the three groups under the best fit ABC model. Times of population size changes are indicated by horizontal dashed lines. Ma, million years ago; NA, ancestral population size; Ne, current population size.

Table 4 Selection of major bioclimatic variables used in this study and their contribution rate to the four time periods considered

		Contribution rate (%)					
Code	Bioclimatic variable	LIG	LGM (CCSM4)	LGM (MIROC)	LGM (MPI-ESM-P)	PRESENT	FUTURE
Bio 2	Mean diurnal range (mean of monthly [max temp – min temp])	0.2	0.8	0.4	2	1.4	0.9
Bio 3	Isothermality	0.9	3.8	4.9	0.8	2	2.7
Bio 8	Mean temperature of wettest quarter	0.3	1	0.8	0.4	0.5	0.6
Bio10	Mean temperature of warmest quarter	13.6	17	14.1	16.7	14.9	13.3
Bio11	Mean temperature of coldest quarter	0.6	0.5	0.5	0.1	0.9	0.9
Bio12	Annual precipitation	18.2	12.2	13.8	22.9	17.3	15.8
Bio15	Precipitation seasonality (coefficient of variation)	2.8	4.3	3.2	2.5	4.5	1.9
Bio16	Precipitation of wettest quarter	0.1	0.4	0.2	0.2	0.1	0.1
Bio19	Precipitation of coldest quarter	63.2	59.9	62	54.4	58.6	63.8

CCSM4, Community Climate System Model Version 4; LGM, Last Glacial Maximum; LIG, Last Interglacial period; MIROC, Model for Interdisciplinary Research on Climate; MPI-ESM-P, New Earth System Model of the Max Planck Institute for Meteorology.

heavy global warming scenario (RCP 8.5; Table 5). The mountains of southeastern China, northern Taiwan Island, and southwestern Japan were depicted as potential across all climate scenarios (Fig. 4). If we try to translate the potential range expansions/contractions to the three detected genetic clusters, most changes corresponded to mainland China, which showed very considerable range contractions from LGM into the future (Fig. 4).

Table 5 Potential suitable areas of *Conandron ramondioides* in different climate scenarios ($\times 10^4$ km^2)

Time	Highly suitable area	Moderately suitable area	Lowly suitable area	Total suitable area	Unsuitable area
LIG	4.34	18.86	35.50	58.70	804.45
LGM (CCSM4)	0.32	5.76	68.82	74.90	790.51
LGM (MIROC)	0.09	13.27	68.52	81.88	783.54
LGM (MPI-ESM-P)	0.36	26.48	71.30	98.14	767.27
PRESENT	2.60	14.76	27.84	45.20	817.94
FUTURE	1.41	11.07	23.41	35.89	827.25

CCSM4, Community Climate System Model Version 4; LGM, Last Glacial Maximum; LIG, Last Interglacial period; MIROC, Model for Interdisciplinary Research on Climate; MPI-ESM-P, New Earth System Model of the Max Planck Institute for Meteorology.

Table 6 Changes in suitable habitat area for *Conandron ramondioides* in different climate scenarios ($\times 10^4$ km^2)

Climate scenario	Range expansion	No occupancy (absence in both)	No change (presence in both)	Range contraction
LGM (CCSM4)–LIG	1.35	701.53	3.71	17.13
LGM (MIROC)–LIG	6.14	696.74	6.17	14.66
LGM (MPI)–LIG	12.04	690.84	12.47	8.36
PRESENT–LIG	0.41	706.20	15.41	5.83
PRESENT–LGM (CCSM4)	12.06	706.60	3.41	1.65
PRESENT–LGM (MIROC)	10.55	700.84	4.92	7.39
PRESENT–LGM (MPI)	5.57	693.63	9.90	14.61
FUTURE–PRESENT	3.41	708.61	7.68	8.15

CCSM4, Community Climate System Model Version 4; LGM, Last Glacial Maximum; LIG, Last Interglacial period; MIROC, Model for Interdisciplinary Research on Climate; MPI-ESM-P, New Earth System Model of the Max Planck Institute for Meteorology.

3.5 Niche comparisons in environment space

Based on 74 input occurrence data (Fig. 5A) and nine climatic variables (bio2, bio3, bio5, bio8, bio10–12, bio16, and bio19), the results showed that the first two components of the PCA-env explained 60.76% of the total climatic variability examined, with PC1 = 32.05% and PC2 = 28.71% (Figs. 5B, 5C). The mean diurnal range (bio2) was the most contributing variable to PC1, whereas bio2, isothermality (bio3) and precipitation in the wettest quarter (bio16) were the variables most intensely associated with PC2. Mainland China and Japan showed very close realized niches, with that of Taiwan Island very distant from them (Figs. 5B, 5C).

A similar pattern was detected by the niche overlap index (Schoener's D_S) (Table 7); the highest D_S values were found between mainland China and Japan ($D_S = 0.201$), followed by those between Japan and Taiwan Island ($D_S = 0.128$), and between mainland China and Taiwan Island ($D_S = 0$). A niche divergence scenario was detected between Taiwan Island and each of the other two clades (mainland China and Japan) by the niche equivalency test (Table 7). However, the niche similarity test, which takes the surrounding areas where the clades occur into account, was not capable of detecting any signal of niche divergence (or niche conservatism) among the three clades.

4 Discussion

Based on population genomic data, a strong population genetic structure was found for the monotypic and relict species *Conandron ramondioides* in the complex and highly fragmented habitats of the Sino-Japanese floristic region (SJFR; Fig. 1). The patterns of phylogeographic structure detected by coalescent analyses were also congruent, and three genetic barriers were identified (Fig. 2C), which captured the main characteristics of population divergence history. Coalescent methods and SDM generally supported the idea that the three genetic groups have survived in various refugia during Quaternary glacial cycles, albeit experiencing several expansions/contractions (Figs. 3, 4), and formed a deep ecological niche divergence among regions (Fig. 5).

4.1 Genetic diversity and phylogeographic pattern

There was very low population-level genetic diversity of *C. ramondioides* (H_E: 0.042–0.062, π: 0.030–0.061) (Table 2) and most gene flow between populations and regions were less than 1 (Table S3). This coincides with former studies in the species using the gene *Gcyc1* (Xiao, 2005; Xiao et al., 2012) and suggests a combined effect of small population sizes, a low success of sexual reproduction, and restricted gene flow in *C. ramondioides*. The AMOVA analysis and F_{ST} values among *C. ramondioides* populations also showed that most genetic variation resides among populations (40.04%) and regions (45.91%), indicating little gene flow between populations and regions. This herb occurs in populations of small size mostly on streamside rocks in valleys under evergreen broad-leaved forests (Xiao et al., 2012); these sites are, in addition, characterized by a high pollen limitation due to low levels of insect visitation (Xiao, 2005; Hsin & Wang, 2018; Ren MX, pers. obs., 2020), although its actinomorphic flowers may help to attract generalized pollinators (Wang et al., 2010; Hsin & Wang, 2018). The

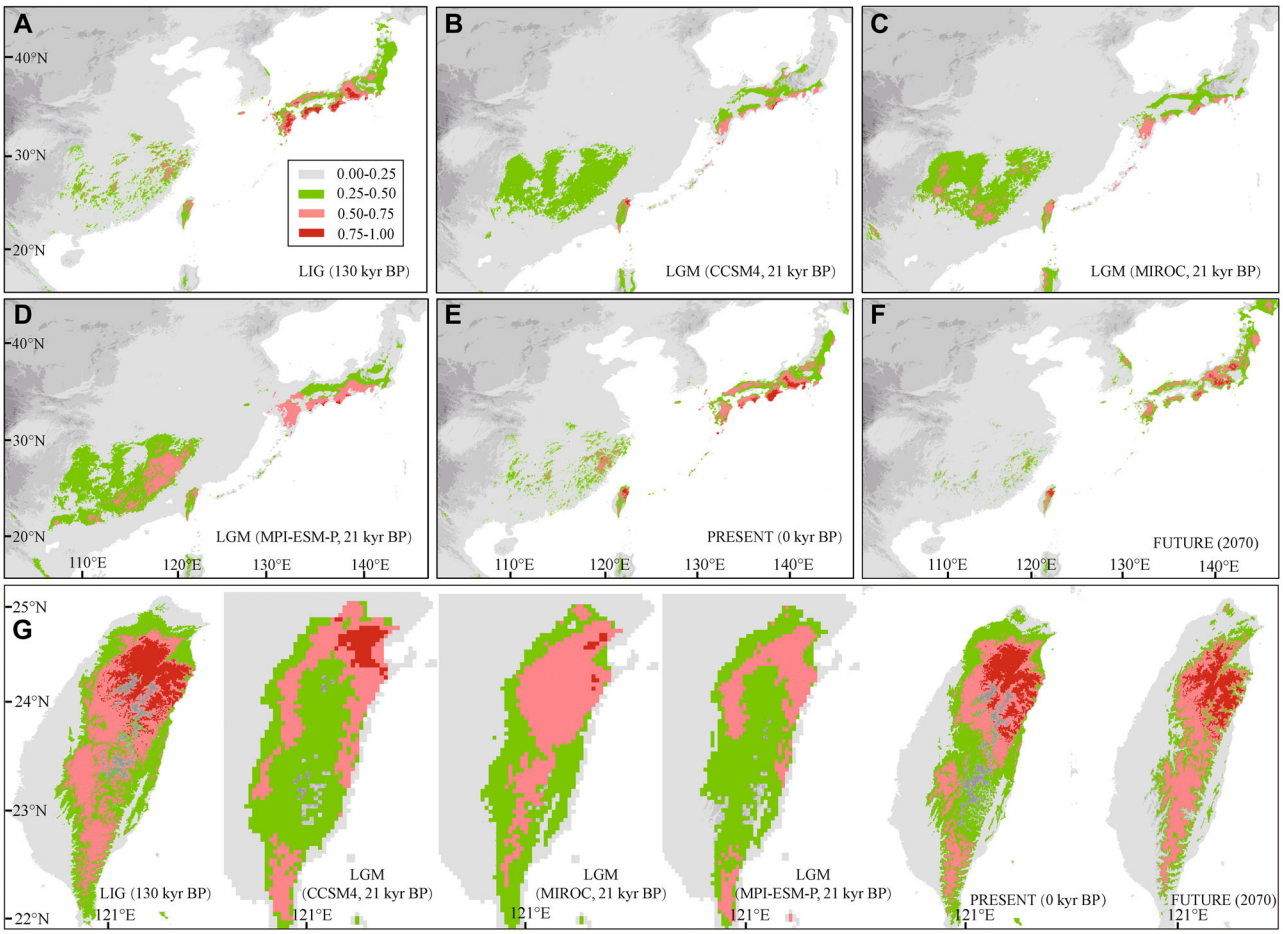

Fig. 4. Results of species distribution modeling (SDM) of *Conandron ramondioides*, represented as predicted distribution probability (as logistic values). **A**, Average projection of the model to the Last Interglacial (ca. 120–140 kyr before present [BP]). Average projections of the model to the Last Glacial Maximum (ca. 21 kyr BP) using the (**B**) Community Climate System Model Version 4 (CCSM4), (**C**) Model for Interdisciplinary Research on Climate (MIROC), and (**D**) New Earth System Model of the Max Planck Institute for Meteorology (MPI-ESM-P) general circulation model simulations. **E**, Predicted distribution for current climatic conditions. **F**, Average projections of the model to the future (2070). **G**, Zoom of SDMs for Taiwan Island. kyr, 1000 years.

isolated nature of *C. ramondioides* habitats (moist rocks) is enhanced by recent human disturbance, including the tourism activities and hydropower development observed in many populations (Wang, 2004; Xiao, 2005; Wang et al., 2010). All these factors combined compromise successful pollination and seed germination, thereby accelerating the rate of genetic erosion within populations via increased inbreeding and genetic drift (Young et al., 1996; Hsin & Wang, 2018), as well as promoting genetic differentiation among populations and regions (Xiao et al., 2012). ADMIXTURE analysis, PCA, and the phylogenetic tree all indicate that there are three distinct genetic lineages within *C. ramondioides*, which correspond to the three main regions where the species is present, that is, mainland China, Taiwan Island, and Japan (Figs. 1, 2B). Hsin (2019), using single-copy nuclear markers, also identified these three genetic clusters, whereas Xiao et al. (2012) also found two genetic clusters for China (i.e., mainland China and Taiwan Island) with the CYCLOIDEA1 (GCYC1) coding sequence. The clear genetic clustering pattern, which has a strong geographic basis, together with a significant positive correlation between genetic distance and geographic distance at the population level ($r = 0.499$, $P = 0.01$; Fig. S3), suggest that geographic isolation is the main reason for genetic differentiation within *C. ramondioides*.

Geographic barriers, such as islands, valleys, and rivers, are often responsible for population differentiation and phylogeographic structure by weakening or blocking gene flow (MacArthur & Wilson, 1967; Li et al., 2011; Robin et al., 2015). Three major genetic barriers have been detected in *C. ramondioides* that coincide with extant large topographic barriers within the species range: the East China Sea, Taiwan Strait, and Tokyo Bay (Fig. 2C). Thus, it is possible to conclude that these landscape interruptions have played an outstanding role in the formation of the phylogeographic structure of this small gesneriad and, thus, in the shaping of its three current genetic clades. Within the Japanese distribution area, one unexpected genetic boundary was

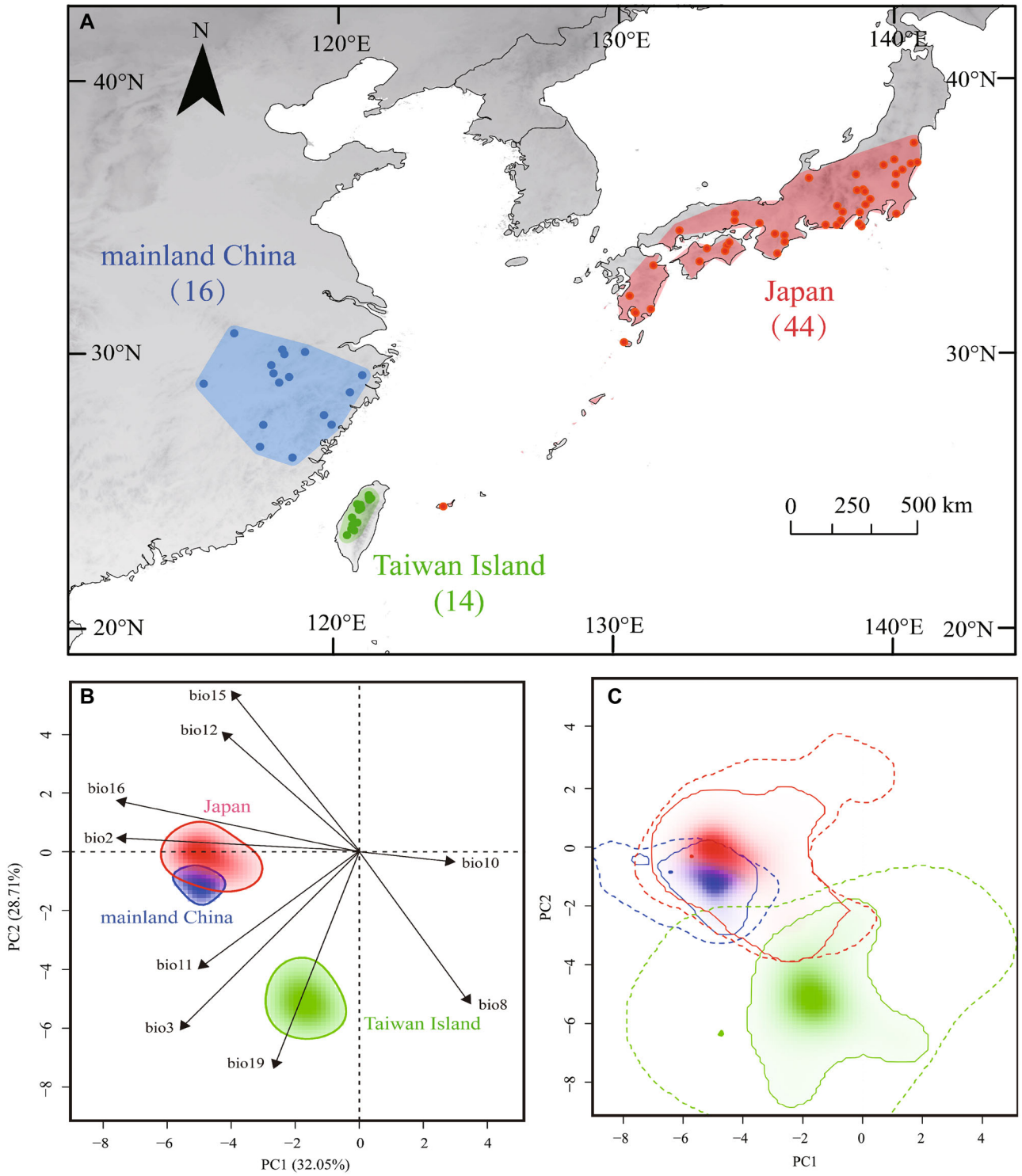

Fig. 5. Niche comparisons in environmental space obtained by the environmental niche analysis in RStudio platform. **A**, Distributional ranges used for the climatic niche evaluation of *Conandron ramondioides* in mainland China (blue), Taiwan Island (green), and Japan (red). The occurrence records were showed by dots, and colored polygons represented the background areas. The number of occurrence records used for each range were showed below the ranges labels. **B, C**, Global climate space, where the three realized niches in a shading gradation scale according to their density of occurrence per cell are projected. **B**, The contribution and direction of the nine climatic variables to the first two principal components analysis of environmental variables (PCA-env) axes are presented, and the solid lines illustrate the 50% of occurrence density. **C**, The solid and dashed lines show the 100% occurrences density and the 100% available climatic background, respectively.

Table 7 Paired niche comparisons between the three distribution ranges examined: *Conandron ramondioides* from mainland China, Taiwan Island, and Japan

Distribution ranges (comparisons 1 → 2)			Equivalency test (*P*-value)		Similarity test (*P*-value)				
1	2	Niche overlap (*Ds*)	Less eq	More eq	Less sim	More sim	Niche unfilling	Niche stability	Niche expansion
Mainland China	Japan	0.201	0.158	0.762	0.871	0.198	0.048	0.371	0.629
	Taiwan Island	0	**0.01D**	1	0.713	1	1	0	1
Japan	Mainland China	0.201	0.277	0.743	0.861	0.149	0.629	0.952	0.048
	Taiwan Island	0.128	**0.03D**	0.99	0.881	0.168	0.931	0.119	0.881
Taiwan Island	Mainland China	0	**0.01D**	1	0.713	1	1	0	1
	Japan	0.128	**0.03D**	1	0.891	0.119	0.881	0.069	0.931

Schoener's *Ds* indicates the niche overlap level between realized climatic niches, 0 = no overlap, 1 = complete overlap. The niche equivalency (eq) and niche similarity (sim) tests are significant ($P < 0.05$) when niche overlap is smaller than randomly expected (niche divergence; D), or larger than randomly expected (niche conservation; C). The three niche dynamic parameters (unfilling, stability, expansion) are also shown.

found at Tokyo Bay (Fig. 2A), which is located at the "Fossa Magna," a great rift in Honshu Island caused by the collision and merging of central and northern Japan ca. 15 Ma (Kato, 1992), and which would have facilitated genetic differentiation between JP-CB and JP-CCB/JP-YD. In addition to the role played by this rift, it should be noted the current Boso Peninsula (where JP-CB is situated) became an island separated from the main Honshu Island during the mid-Pleistocene period (Shimizu & Ueshima, 2000; Kase et al., 2013), where populations JP-CCB and JP-YD occur. Therefore, the JP-CB population may have experienced further geographic isolation with respect to JP-CCB and JP-YD populations, thus accumulating distinctive genetic variation (note the much longer branch of JP-CB in the phylogeny of Fig. 2B). Other studies with Japanese native species also found substantial genetic divergence between northern and central regions in Honshu, including plants (Senni et al., 2005; Ikeda et al., 2006; Hiraoka & Tomaru, 2009; Qiu et al., 2009), insects (Sota & Hayashi, 2007; Schoville et al., 2013; Saito & Tojo, 2016), and vertebrates (Oshida et al., 2009; Setiamarga et al., 2009; Nunome et al., 2010).

4.2 Historical demography

As an East Asian endemic lineage, *Conandron* is, strangely, phylogenetically close to the Southeast Asian *Ridleyandra* (Roalson & Roberts, 2016). These two genera are taxonomically placed within the Didymocarpoid Gesneriaceae (Weber, 2004), one of the most ancient groups in the family, whose origin lies between late Cretaceous (69.66 Ma [48.20–77.06]; Roalson & Roberts, 2016) and middle Eocene (44.70 Ma [37.10–60.50]; Perret et al., 2013). The crown age of *Conandron* is estimated to be ca. 30 Ma in the late Oligocene period, confirming the monotypic *Conandron* as a relict lineage in East Asia.

The DIYABC analyses suggested that Scenario 4 was the best fit model based on genomic data, which showed that Group MC and Group JP originated from an uncertain common ancestor (Group MC + JP; Fig. 3A), and Group TW originated from Group MC. As a relict plant, the ancestral lineage of *C. ramondioides* would have expanded a long time ago across the whole SJFR and became fragmented much later, probably as a consequence of orogenic movements in East Asia. First, Japanese islands separated from continental eastern Asia during the mid-Miocene opening of the Sea of Japan (22–15 Ma; Barnes, 2003; Schoville et al., 2013; Saito & Tojo, 2016), which offered the opportunities for population divergence of *Paris japonica* (Franch. and Sav.) Franch. (Yang et al., 2019), *Galium* L. (Jeong et al., 2016) and *Neolitsea sericea* (Blume) Koidz. (Lee et al., 2013). According to our results, Group MC and Group JP began to diverge at ca. 11.850 Ma (95% CI: 6.180–15.660 Ma), which suggests that the formation of the Sea of Japan would have driven genetic isolation between the two sides of the sea. Certainly, the divergence between Groups MC and JP would have taken place before the first formation of the East China Sea land bridge (7.0–5.0 Ma; Kimura, 2003), which connected Japan with the continent again. Second, Taiwan Island was formed more recently, after orogenic movements generated by the collision of the Philippine Sea Plate and the Eurasia plate at ca. 9 Ma, in the late Miocene period (Sibuet & Hsu, 2004).

Subsequently, the orogeny of the Central Range in Taiwan Island at ca. 5–6 Ma created many new habitats, thus promoting the formation of Taiwan flora in the late Miocene and early Pliocene periods (Sibuet & Hsu, 2004). Such tectonic events would have facilitated the dispersal of *C. ramondioides* from mainland China and its establishment in Taiwan Island shortly after (ca. 4.050 Ma, 95% CI: 2.601–7.410 Ma). Therefore, both diversification events would have occurred just before the Quaternary. The same branching order was also found by Hsin (2019), although with different tempos: ca. 1.13 Ma (95% CI: 0.26–1.80 Ma) for the first diversification event between Group MC and Group JP, and 0.75 Ma (95% CI: 0.37–1.00 Ma) for the second diversification event between Group MC and Group TW; this time disparity with respect to our results may be due to the small number of mutant nucleotide sites used in the previous study of Hsin (2019).

The emergence and rapid uplift of Taiwan Island, with an active orogeny that resulted in Taiwan's Central Mountain Range, made available many new niches that *C. ramondioides* could explore. The niche comparison among the genetic clades shows that Taiwan's range occupies a considerably different climatic space, particularly regarding the occurrences (but also partly for the background; Fig. 5), which may indicate a progressing evolutionary niche shift and climatic specialization after the dispersal of *C. ramondioides* from mainland China to Taiwan Island in early Pliocene. Similarly, an ecological niche divergence scenario was found between *Cypripedium formosanum* Hayata (endemic to Taiwan Island) and its relative *C. japonicum* Thunb. (widespread in mainland China, Korea, and Japan) (Han et al., 2022). In contrast, the strong genetic differentiation between mainland Chinese and Japanese populations cannot be translated to the climatic niche, probably because they share the same climatic background (Fig. 5).

It is generally acknowledged that climatic fluctuations during the Pleistocene had a dramatic effect on phylogeographic patterns and demographic history of plant species (Comes & Kadereit, 1998; Hewitt, 2004), especially for the cold-adapted montane species distributed in the SJFR that are particularly vulnerable to past climatic changes (Sun et al., 2014; Xia et al., 2022). Our demographic models show that Group TW, once diverged from Group MC, would have experienced a population contraction at ca. 1.653 Ma (95% CI: 0.453–2.934 Ma), followed by an expansion at ca. 0.166 Ma (95% CI: 0.049–0.289 Ma) (Fig. 3B). Group MC experienced a large population contraction at ca. 1.755 Ma (95% CI: 0.690–2.613 Ma), while Group JP maintained a more or less stable population size before the late Pleistocene, with the exception of a recent bottleneck from ca. 0.804 Ma (95% CI: 0.471–1.116 kyr) to ca. 0.193 Ma (95% CI: 0.036–0.289 Ma). Population contractions for TW and MC at ca. 1.7 Ma, and for JP at 0.8 Ma are not casual; rather, they may be linked to the deterioration of climate conditions at the onset of the Calabrian period and the end of the mid-Pleistocene transition, respectively. These climatic changes produced the decline and extirpation of several relict lineages from Europe, where very accurate pollen and plant macrofossil records are available. For example, *Taxodium* Rich. started to decline in Greece at ca. 1.8 Ma, while *Eucommia* Oliv. disappeared from Spain and France ca. 0.8 Ma, and *Cathaya* Chun and Kuang and *Tsuga* Carr. from southern Italy and northern Italy, respectively, at ca. 0.75 Ma (Magri et al., 2017).

In contrast with Europe and also in North America, where the late Neogene much harsher climatic conditions did not allow most thermophilic elements to survive (Latham & Ricklefs, 1993; Manchester et al., 2009), the large and rather continuous mountain systems in East China (including Taiwan Island) and Japan offered extensive stable but fragmented habitats, likely serving as long-term stable refugia for *C. ramondioides* and other East Asia relict plant in the humid subtropical/warm-temperate areas (López-Pujol et al., 2011; Tang et al., 2018). Even in the LGM, large areas would have been suitable for *C. ramondioides* (Fig. 4).

4.3 Dispersal vs. vicariance in East Asia

Our genetic data of *C. ramondioides* indicate a strong phylogeographic structure consisting of three genetic clusters that have a strong geographical basis (Fig. 1). After Japanese islands separated from continental eastern Asia during the mid-Miocene, the East China Sea land bridge reconnected mainland China and Japan during several periods (7.0–5.0 Ma; 2.0–1.3 Ma, and the glacial cycles during the period 0.2–0.015 Ma; Kimura, 2003). The frequent connection provided by the land bridge offered opportunities for the dispersal of plants (Chung, 2007; Qi et al., 2012; Sakaguchi et al., 2012; Jiang et al., 2021), but this not always offered suitable habitats (i.e., acting as a "filter"; Qiu et al., 2011; Qi et al., 2014). For *C. ramondioides*, the East China Sea land bridge would not have enabled enough gene flow to prevent the strong divergence detected in the present study, which could be due to the lack of suitable habitats throughout most of the land bridges in the glacial periods (Fig. 4).

The Taiwan flora may have its origin in mainland China, the Ryukyu Islands, and tropical Asian regions (Philippines or Vietnam) during the late Miocene and early Pliocene periods (Hsieh, 2003; Chiang & Schaal, 2006). Our demographic models show that the Taiwanese populations of *C. ramondioides* likely originated from Group MC instead of Group JP (at ca. 4.050 Ma), in agreement with other plants of the SJFR (e.g., *Paris japonica*; Yang et al., 2019), but contrary to other examples such as *Trochodendron aralioides* Sieb. and Zucc. (which dispersed from Japan to Taiwan Island throughout the Ryukyu Islands; Huang et al., 2004). In addition, formed by the uplift of Taiwan Island since the Pliocene (Yu & Chou, 2001; Yu, 2003), the Taiwan Strait has acted as a primary genetic barrier between the mainland and the island in many plants (Ruan et al., 2013; Ge et al., 2015), including relict ones (Chou et al., 2011; Qiu et al., 2017). This seems to be also the case for *C. ramondioides*, even though most of the Taiwan Strait would have been passable during the cold periods of the Quaternary (since 2 Ma, marine regressions at glacial maxima reached at least –70 m; Miller et al., 2005).

5 Conclusions

This is the first time that the Tertiary relict plant *Conandron ramondioides*, distributed in mainland China, Taiwan Island, and Japan, has been used as a case study to shed light on the relative roles of dispersal vs. vicariance processes in Sino-Japanese plant disjunctions. The reconstruction of the

phylogeographical relationships and population history within *C. ramondioides*, alongside the species distribution models, highlight the predominance of vicariance processes to explain the current distribution of this relict plant, with three distinct genetic lineages corresponding to three well defined different geographical regions. The sharp genetic differentiation among the three clusters of *C. ramondioides* would be due to low levels of historical gene flow, associated with a long history of geographical isolation before the Quaternary. Our results indicate that RAD-seq methods can be used successfully to examine patterns of historical phylogeography and to assess the relative roles of dispersal and vicariance in species disjunctions. We suggest, nevertheless, that a taxonomic survey with more extensive sampling and detailed morphological comparisons is needed in order to assess whether the three distinct geographically and genetically isolated lineages might represent three subspecies or even cryptic species by constituting a *C. ramondioides* complex. Indeed, two varieties based on morphological characters have been recognized: var. *ramondioides* and var. *taiwanensis* based on studied plants from Japan and Taiwan Island, respectively (Kokubugata & Peng, 2004). The seemingly diverging niche of the Taiwanese clade with respect to that of Japan (and mainland China) clade (s) supports this distinction.

Acknowledgments

We thank Xiang-Wen Hou and Zi-Yun Ren for assistance in fieldwork and Xuan Jin and Yuan-Mi Wu for their assistance in data analysis. Financial support was provided by the National Natural Science Foundation of China (41871041).

Author Contributions

Ming-Xun Ren applied for funding, organized sampling, and designed the study. Ming-Xun Ren conceived the study and collected all samples in Japan. Ke Tan contributed to the demographic analyses. Xiao-Lan Yao contributed to the climatic niche difference analyses and revised the manuscript. Shao-Jun Ling carried out molecular experiments and led the bioinformatics and statistical analysis, prepared figures, and wrote the draft with contributions from Ming-Xun Ren, Jordi López-Pujol, and Juli Caujapé-Castells.

Conflict of Interest

There is no conflict of interest.

Data Availability Statement

The demultiplexed fastq data are archived in NCBI SRA (BioProject ID: PRJNA821665).

References

Aiello-Lammens ME, Boria RA, Radosavljevic A, Vilela B, Anderson RP. 2015. spThin: An R package for spatial thinning of species occurrence records for use in ecological niche models. *Ecography* 38: 541–545.

Alexander DH, Novembre J, Lange K. 2009. Fast model-based estimation of ancestry in unrelated individuals. *Genome Research* 19: 1655–1664.

Baldwin RA. 2009. Use of maximum entropy modeling in wildlife research. *Entropy* 11: 854–866.

Barnes GL. 2003. Origins of the Japanese Islands: The new "Big Picture". *Japan Review* 15: 3–50.

Broennimann O, Di Cola V, Petitpierre B, Breiner F, Scherrer D, D' Amen M, Randin C, Engler R, Hordijk W, Mod H, Pottier J, Di Febbraro M, Pellissier L, Pio D, Garcia-Mateo R, Dubuis A, Maiorano L, Psomas A, Ndiribe C, Salamin N, Zimmermann N, Guisan A. 2014. Package 'ecospat' [online]. Available from https://cran.r-project.org/web/packages/ecospat/index.html [accessed 10 October 2014].

Broennimann O, Fitzpatrick MC, Pearman PB, Petitpierre B, Pellissier L, Yoccoz NG, Thuiller W, Fortin MJ, Randin C, Zimmermann NE, Graham CH, Guisan A. 2012. Measuring ecological niche overlap from occurrence and spatial environmental data. *Global Ecology and Biogeography* 21: 481–497.

Catchen J, Hohenlohe PA, Bassham S, Amores A, Cresko WA. 2013. Stacks: An analysis tool set for population genomics. *Molecular Ecology* 22: 3124–3140.

Caujapé-Castells J, García-Verdugo C, Marrero-Rodríguez Á, Fernández-Palacios JM, Crawford DJ, Mort ME. 2017. Island ontogenies, syngameons, and the origins and evolution of genetic diversity in the Canarian endemic flora. *Perspectives in Plant Ecology, Ecology and Systematics* 27: 9–22.

Chiang YC, Schaal BA. 2006. Phylogeography of plants in Taiwan and the Ryukyu Archipelago. *Taxon* 55: 31–41.

Chou YW, Thomas PI, Ge XJ, LePage BA, Wang CN. 2011. Refugia and phylogeography of *Taiwania* in East Asia. *Journal of Biogeography* 38: 1992–2005.

Chung CH. 2007. Vegetation response to climate change on Jeju Island, South Korea, during the last deglaciation based on pollen record. *Geosciences Journal* 11: 147–155.

Collins M, Knutti R, Arblaster J, Dufresne JL, Fichefet T, Friedlingstein P, Gao XJ, Gutowski WJ, Johns T, Krinner G, Shongwe M, Tebaldi C, Weaver AJ, Wehner MF, Allen MR, Andrews T, Beyerle U, Bitz CM, Bony S, Booth BBB. 2013. Long-term climate change: Projections, commitments and irreversibility. In: Stocker TF, Qin D, Plattner GK, Tignor MMB, Allen SK, Boschung J, Nauels A, Xia Y, Bex V, Midgley PM eds. *Climate change 2013 - The physical science basis: Contribution of working group I to the fifth assessment report of the intergovernmental panel on climate change*. New York: Cambridge University Press. 1029–1136.

Comes HP, Kadereit JW. 1998. The effect of Quaternary climatic changes on plant distribution and evolution. *Trends in Plant Science* 3: 432–438.

Cornuet JM, Pudlo P, Veyssier J, Dehne-Garcia A, Gautier M, Leblois R, Marin JM, Estoup A. 2014. DIYABC v2.0: A software to make approximate Bayesian computation inferences about population history using single nucleotide polymorphism, DNA sequence and microsatellite data. *Bioinformatics* 30: 1187–1189.

Cornuet JM, Ravigné V, Estoup A. 2010. Inference on population history and model checking using DNA sequence and microsatellite data with the software DIYABC (v1.0). *BMC Bioinformatics* 11: 401.

Danecek P, Auton A, Abecasis G, Albers CA, Banks E, DePristo MA, Handsaker RE, Lunter G, Marth GT, Sherry ST, McVean G, Durbin R. 2011. The variant call format and VCFtools. *Bioinformatics* 27: 2156–2158.

Decker JE, McKay SD, Rolf MM, Kim J, Alcalá AM, Sonstegard TS, Hanotte O, Götherström A, Seabury CM, Praharani L, Babar ME, de Almeida Regitano LC, Yildiz MA, Heaton MP, Liu WS, Lei CZ, Reecy JM, Saif-Ur-Rehman M, Schnabel RD, Taylor JF. 2014. Worldwide patterns of ancestry, divergence, and admixture in domesticated cattle. *PLoS Genetics* 10: e1004254.

Doyle JJ, Doyle JL. 1987. A rapid DNA isolation procedure for small quantities of fresh leaf tissues. *Phytochemical Bulletin* 19: 11–15.

Excoffier L, Lischer HE. 2010. Arlequin suite ver 3.5: A new series of programs to perform population genetics analyses under Linux and Windows. *Molecular Ecology Resources* 10: 564–567.

Fielding AH, Bell JF. 1997. A review of methods for the assessment of prediction errors in conservation presence/absence models. *Environmental Conservation* 24: 38–49.

Ge XJ, Hung KH, Ko YZ, Hsu TW, Gong X, Chiang TY, Chiang YC. 2015. Genetic divergence and biogeographical patterns in *Amentotaxus argotaenia* specise complex. *Plant Molecular Biology Reporter* 33: 264–280.

Gent PR, Danabasoglu G, Donner LJ, Holland MM, Hunke EC, Jayne SR, Lawrence DM, Neale R, Rasch PJ, Vertenstein M, Worley P, Yang ZL, Zhang MH. 2011. The community climate system model version 4. *Journal of Climate* 24: 4973–4991.

Han LX, Jin Y, Zhang JL, Li XL, Chung MY, Herrando-Moraira S, Kawahara T, Yukawa T, Chung SW, Chung JM, Kim YD, López-Pujol J, Chung MG, Tian HZ. 2022. Phylogeography of the endangered orchids *Cypripedium japonicum* and *Cypripedium formosanum* in East Asia: Deep divergence at infra- and interspecific levels. *Taxon* 71: 733–757.

Herrando-Moraira S, Nualart N, Herrando-Moraira A, Chung MY, Chung MG, López-Pujol J. 2019. Climatic niche characteristics of native and invasive *Lilium lancifolium*. *Scientific Reports* 9: 14334.

Hewitt GM. 2004. Genetic consequences of climatic oscillations in the Quaternary. *Philosophical Transactions of the Royal Society B: Biological Sciences* 359: 183–195.

Hijmans RJ, Cameron SE, Parra JL, Jones PG, Jarvis A. 2005. Very high resolution interpolated climate surfaces for global land areas. *International Journal of Climatology* 25: 1965–1978.

Hiraoka K, Tomaru N. 2009. Genetic divergence in nuclear genomes between populations of *Fagus crenata* along the Japan Sea and Pacific sides of Japan. *Journal of Plant Research* 122: 269–282.

Hsieh CF. 2003. Composition, endemism and phytogeographical affinities of the Taiwan flora. In: Editorial Committee of the Flora of Taiwan eds. *Flora of Taiwan*. Taipei: Department of Botany, National Taiwan University. 2: 1–14.

Hsin KT. 2019. *Phylogeography, flower development and selection on floral symmetry gene in East Asia endemic Conandron ramondioides*. Ph.D. Dissertation. Taipei: National Taiwan University.

Hsin KT, Wang CN. 2018. Expression shifts of floral symmetry genes correlate to flower actinomorphy in East Asia endemic *Conandron ramondioides* (Gesneriaceae). *Botanical Studies* 59: 24.

Huang SF, Hwang SY, Wang JC, Lin TP. 2004. Phylogeography of *Trochodendron aralioides* (Trochodendraceae) in Taiwan and its adjacent areas. *Journal of Biogeography* 31: 1251–1259.

Hudson RR. 2002. Generating samples under a Wright-Fisher neutral model of genetic variation. *Bioinformatics* 18: 337–338.

Ikeda H, Senni K, Fujii N, Setoguchi H. 2006. Refugia of *Potentilla matsumurae* (Rosaceae) located at high mountains in the Japanese archipelago. *Molecular Ecology* 15: 3731–3740.

Jeong KS, Shin JK, Maki M, Pak JH. 2016. Phylogeny of *Galium* L. (Rubiaceae) from Korea and Japan based on chloroplast DNA sequence. *Bangladesh Journal of Plant Taxonomy* 23: 237–246.

Jiang K, Tong X, Ding YQ, Wang ZW, Miao LY, Xiao YE, Huang WC, Hu YH, Chen XY. 2021. Shifting roles of the East China Sea in the phylogeography of red nanmu in East Asia. *Journal of Biogeography* 48: 2486–2501.

Jombart T. 2008. Adegenet: a R package for the multivariate analysis of genetic markers. *Bioinformatics* 24: 1403–1405.

Kase T, Nakano T, Kurihara Y, Haga T. 2013. A middle Pleistocene limpet assemblage from central Japan (Gastropoda: Patellogastropoda) and selective extinction of intertidal rocky shore molluscs in response to glacio-eustatic sea-level changes. *Paleontological Research* 17: 261–281.

Kato H. 1992. Fossa Magna—A masked border region separating southwest and northeast Japan. *Bulletin of the Geological Survey of Japan* 43: 1–30.

Kimura M. 2003. Land connections between Eurasian continent and Japanese Islands-related to human migration. *Migration & Diffusion* 4: 14–33.

Kokubugata G, Peng CI. 2004. Floral morphology and recognition of varieties in *Conandron ramondioides* (Gesneriaceae) from Japan and Taiwan. *Edinburgh Journal of Botany* 61: 21–30.

Latham RE, Ricklefs RE. 1993. Continental comparisons of temperate-zone tree species diversity. In: Ricklefs RE, Schluter D eds. *Species diversity in ecological communities*. Chicago: University Chicago Press. 294–314.

Lee JH, Lee DH, Choi BH. 2013. Phylogeography and genetic diversity of East Asian *Neolitsea sericea* (Lauraceae) based on variations in chloroplast DNA sequences. *Journal of Plant Research* 126: 193–202.

Li Y, Zhai SN, Qiu YX, Guo YP, Ge XJ, Comes HP. 2011. Glacial survival east and west of the "Mekong–Salween Divide" in the Himalaya–Hengduan Mountains region as revealed by AFLPs and cpDNA sequence variation in *Sinopodophyllum hexandrum* (Berberidaceae). *Molecular Phylogenetics and Evolution* 59: 412–424.

Lischer HEL, Excoffier L. 2012. PGDSpider: An automated data conversion tool for connecting population genetics and genomics programs. *Bioinformatics* 28: 298–299.

López-Pujol J, Zhang FM, Sun HQ, Ying TS, Ge S. 2011. Centres of plant endemism in China: Places for survival or for speciation? *Journal of Biogeography* 38: 1267–1280.

MacArthur RH, Wilson EO. 1967. *The theory of island biogeography*. Princeton: Princeton University Press.

Magri D, Di Rita F, Aranbarri J, Fletcher W, González-Sampériz P. 2017. Quaternary disappearance of tree taxa from Southern Europe: Timing and trends. *Quaternary Science Reviews* 163: 23–55.

Manchester SR, Chen ZD, Lu AM, Uemura K. 2009. Eastern Asian endemic seed plant genera and their paleogeographic history throughout the Northern Hemisphere. *Journal of Systematics and Evolution* 47: 1–42.

Manni F, Guerard E, Heyer E. 2004. Geographic patterns of (genetic, morphologic, linguistic) variation: How barriers can be detected by using Monmonier's algorithm. *Human Biology* 76: 173–190.

Miller KG, Kominz MA, Browning JV, Wright JD, Mountain GS, Katz ME, Sugarman PJ, Cramer BS, Christie-Black N, Pekar SF. 2005. The Phanerozoic record of global sea-level change. *Science* 310: 1293–1298.

Monmonier M. 1973. Maximum-difference barriers: An alternative numerical regionlization method. *Geographical Analysis* 5: 245–261.

Nunome M, Torii H, Matsuki R, Kinoshita G, Suzuki H. 2010. The influence of Pleistocene refugia on the evolutionary history of

the Japanese hare, *Lepus brachyurus*. *Zoological science* 27: 746–754.

Oshida T, Masuda R, Ikeda K. 2009. Phylogeography of the Japanese giant flying squirrel, *Petaurista leucogenys* (Rodentia: Sciuridae): Implication of glacial refugia in an arboreal small mammal in the Japanese Islands. *Biological Journal of the Linnean Society* 98: 47–60.

Otto-Bliesner BL, Marshall SJ, Overpeck JT, Miller GH, Hu AX. 2006. Simulating Arctic climate warmth and icefield retreat in the Last Interglaciation. *Science* 311: 1751–1753.

Perret M, Chautems A, de Araujo AO, Salamin N. 2013. Temporal and spatial origin of Gesneriaceae in the New World inferred from plastid DNA sequences. *Biological Journal of the Linnean Society* 171: 61–79.

Phillips SJ, Anderson RP, Schapire RE. 2006. Maximum entropy modeling of species geographic distributions. *Ecological Modelling* 190: 231–259.

Qi XS, Chen C, Comes HP, Sakaguchi S, Liu YH, Tanaka N, Sakio H, Qiu YX. 2012. Molecular data and ecological niche modelling reveal a highly dynamic evolutionary history of the East Asian Tertiary relict *Cercidiphyllum* (Cercidiphyllaceae). *New Phytologist* 196: 617–630.

Qi XS, Yuan N, Comes HP, Sakaguchi S, Qiu YX. 2014. A strong "filter" effect of the East China Sea land bridge for East Asia's temperate plant species: Inferences from molecular phylogeography and ecological niche modelling of *Platycrater arguta* (Hydrangeaceae). *BMC Evolutionary Biology* 14: 41.

Qiu YX, Fu CX, Comes HP. 2011. Plant molecular phylogeography in China and adjacent regions: Tracing the genetic imprints of Quaternary climate and environmental change in the world's most diverse temperate flora. *Molecular Phylogenetics and Evolution* 59: 225–244.

Qiu YX, Lu QX, Zhang YH, Cao YN. 2017. Phylogeography of East Asia's tertiary relict plants: Current progress and future prospects. *Biodiversity Science* 25: 136–146.

Qiu YX, Qi XS, Jin XF, Tao XY, Fu CX, Naiki A, Comes HP. 2009. Population genetic structure, phylogeography, and demographic history of *Platycrater arguta* (Hydrangeaceae) endemic to east China and south Japan, inferred from chloroplast DNA sequence variation. *Taxon* 58: 1226–1241.

R Core Team. 2021. R: A language and environment for statistical computing. Vienna: R Foundation for Statistical Computing. Available from https://www.R-project.org/

Roalson EH, Roberts WR. 2016. Distinct processes drive diversification in different clades of Gesneriaceae. *Systematic Biology* 65: 662–684.

Robin VV, Vishnudas CK, Gupta P, Ramakrishnan U. 2015. Deep and wide valleys drive nested phylogeographic patterns across a montane bird community. *Proceedings of the Royal Society B: Biological Sciences* 282: 20150861.

Ruan Y, Huang BH, Lai SJ, Wan YT, Li JQ, Huang S, Liao PC. 2013. Population genetic structure, local adaptation, and conservation genetics of *Kandelia obovata*. *Tree Genetics & Genomes* 9: 913–925.

Saito R, Tojo K. 2016. Complex geographic- and habitat-based niche partitioning of an East Asian habitat generalist mayfly *Isonychia japonica* (Ephemeroptera: Isonychiidae) with reference to differences in genetic structure. *Freshwater Science* 35: 712–723.

Sakaguchi S, Qiu YX, Liu YH, Qi XS, Kim SH, Han JY, Takeuchi Y, Worth JRP, Isagi YJ. 2012. Climate oscillation during the Quaternary associated with landscape heterogeneity promoted allopatric lineage divergence of a temperate tree *Kalopanax septemlobus* (Araliaceae) in East Asia. *Molecular Ecology* 21: 3823–3838.

Schoener TW. 1970. Nonsynchronous spatial overlap of lizards in patchy habitats. *Ecology* 51: 408–418.

Schoville SD, Uchifune T, Machida R. 2013. Colliding fragment islands transport independent lineages of endemic rock-crawlers (Grylloblattodea: Grylloblattidae) in the Japanese archipelago. *Molecular Phylogenetics and Evolution* 66: 915–927.

Senni K, Fujii N, Takahashi H, Sugawara T, Wakabayashi M. 2005. Intraspecific chloroplast DNA variations of the alpine plants in Japan. *Acta Phytotaxonomica et Geobotanica* 56: 265–275.

Setiamarga DHE, Miya M, Yamanoue Y, Azuma Y, Inoue JG, Ishiguro NB, Mabuchi K, Nishida M. 2009. Divergence time of the two regional medaka populations in Japan as a new time scale for comparative genomics of vertebrates. *Biology Letters* 5: 812–816.

Shimizu Y, Ueshima R. 2000. Historical biogeography and interspecific mtDNA introgression in *Euhadra peliomphala* (the Japanese land snail). *Heredity* 85: 84–96.

Sibuet JC, Hsu SK. 2004. How was Taiwan created? *Tectonophysics* 379: 159–181.

Silva DP, Vilela B, Buzatto BA, Moczek AP, Hortal J. 2016. Contextualized niche shifts upon independent invasions by the dung beetle *Onthophagus taurus*. *Biological Invasions* 18: 3137–3148.

Sota T, Hayashi M. 2007. Comparative historical biogeography of *Plateumaris* leaf beetles (Coleoptera: Chrysomelidae) in Japan: Interplay between fossil and molecular data. *Journal of Biogeography* 34: 977–993.

Stamatakis A. 2006. RaxML-VI-HPC: Maximum likelihood-based phylogenetic analyses with thousands of taxa and mixed models. *Bioinformatics* 22: 2688–2690.

Sun YX, Moore MJ, Yue LL, Feng T, Chu HJ, Chen ST, Ji YH, Wang HC, Li JQ. 2014. Chloroplast phylogeography of the East Asian Arcto-Tertiary relict *Tetracentron sinense* (Trochodendraceae). *Journal of Biogeography* 41: 1721–1732.

Swets JA. 1988. Measuring the accuracy of diagnostic systems. *Science* 240: 1285–1293.

Tallis JH. 1991. *Plant community history: Long-term changes in plant distribution and diversity*. London: Chapman and Hall.

Tang CQ, Matsui T, Ohashi H, Dong YF, Momohara A, Herrando-Moraira A, Qian SH, Yang YC, Ohsawa M, Luu HT, Grote PJ, Krestov PV, LePage B, Werger M, Robertson K, Hobohm C, Wang CY, Peng MC, Chen X, Wang HC, Su WH, Zhou R, Li SF, He LY, Yan K, Zhu MY, Hu J, Yang RH, Li WH, Tomita M, Wu ZL, Yan HZ, Zhang GF, He H, Yi SR, Gong HD, Song K, Song D, Li XS, Zhang ZY, Han PB, Shen LQ, Huang DS, Luo K, López-Pujol J. 2018. Identifying long-term stable refugia for relict plant species in East Asia. *Nature Communications* 9: 4488.

Wang WT, Pan KY, Li ZY, Weitzman AL, Skog LE. 1998. Gesneriaceae. In: Wu ZY, Raven PH, Hong DY eds. *Flora of China*. Beijing: Science Press; St. Louis: Missouri Botanical Garden Press. 18: 244–401.

Wang YS, Xie BY, Wan FH, Xiao QM, Dai LY. 2007. Application of ROC curve analysis in evaluating the performance of alien species' potential distribution models. *Biodiversity Science* 15: 365–372.

Wang YZ. 2004. Conandron. In: Li ZY, Wang YZ eds. *Plants of Gesneriaceae in China*. Zhengzhou: Henan Science and Technology Publishing House. 3–7.

Wang YZ, Liang RH, Wang BH, Li JM, Qiu ZJ, Li ZY, Weber A. 2010. Origin and phylogenetic relationships of the Old World Gesneriaceae with actinomorphic flowers, inferred from ITS and *trn*L-*trn*F sequences. *Taxon* 59: 1044–1052.

Warren DL, Glor RE, Turelli M. 2008. Environmental niche equivalency versus conservatism: Quantitative approaches to niche evolution. *Evolution* 62: 2868–2883.

Watanabe S, Hajima T, Sudo K, Nagashima T, Takemura T, Okajima H, Nozawa T, Kawase H, Abe M, Yokohata T, Ise T, Sato H, Kato E, Takata K, Emori S, Kawamiya M. 2011. MIROC-ESM 2010: Model description and basic results of CMIP5-20c3m experiments. *Geoscientific Model Development Discussions* 4: 1063–1128.

Weber A. 2004. Gesneriaceae. In: Kubitzki K, Kadereit J eds. *The families and genera of vascular plants*. Berlin/Heidelberg: Springer. 7: 63–158.

Wright S. 1951. The genetical structure of populations. *Nature* 15: 323–354.

Xia XM, Yang MQ, Li CL, Huang SX, Jin WT, Shen TT, Wang F, Li XH, Yoichi W, Zhang LH, Zheng YR, Wang XQ. 2022. Spatiotemporal evolution of the global species diversity of *Rhododendron*. *Molecular Biology and Evolution* 39: msab314.

Xiao LH. 2005. *Studies on molecular ecology and evolution of Conandron ramondioides (Gesneriaceae) populations*. Master Dissertation. Hohhot: Inner Mongolia University.

Xiao LH, Li Z, Wang R, Wang YZ. 2012. Population differentiation and phylogeographic pattern of a relict species, *Conandron ramondioides* (Gesneriaceae), revealed from sequence polymorphism and haplotypes of the *CYCLOIDEA* gene. *Journal of Systematics and Evolution* 50: 45–57.

Yamazaki T. 1993. Gesneriaceae. In: Iwatsuki K, Yamazaki T, Boufford DE, Ohba H eds. *Flora of Japan*. Tokyo: Kodansha. IIIa: 376–379.

Yang LF, Yang ZY, Liu CK, He ZS, Zhang ZR, Yang J, Liu HY, Yang JB, Ji YH. 2019. Chloroplast phylogenomic analysis provides insights into the evolution of the largest eukaryotic genome holder, *Paris japonica* (Melanthiaceae). *BMC Plant Biology* 19: 293.

Young A, Boyle T, Brown T. 1996. The population genetic consequences of habitat fragmentation for plants. *Trends in Ecology and Evolution* 11: 413–418.

Yu HS. 2003. Geological characteristics and distribution of submarine physiographic features in the Taiwan region. *Marine Georesources & Geotechnology* 21: 139–153.

Yu HS, Chou YW. 2001. Physiographic and geological characteristics of shelves in north and west of Taiwan. *Science in China (Series D)* 44: 696–707.

Supplementary Material

The following supplementary material is available online for this article at http://onlinelibrary.wiley.com/doi/10.1111/jse.12937/suppinfo:

Table S1. Locations of *Conandron ramondioides* used in species distribution modeling.

Table S2. Pairwise comparison of F_{ST} values (below diagonal) and geographic distance (m) (above diagonal) among *Conandron ramondioides* populations.

Table S3. Pairwise comparison of gene flow (*Nm* values) among *Conandron ramondioides* populations.

Table S4. DIYABC parameter estimation for all the best-fitting scenarios of divergence and demography model. The q025 and q975 referred to upper and lower limit of the 95% confidence interval value.

Fig. S1. A, Divergence scenarios and corresponding posterior probabilities of *Conandron ramondioides* from DIYABC. In Scenario 1, Group TW was originated from Group MC and diverged at T1, Group MC was originated from Group JP (ancestral population) and diverged at T2; In Scenario 2, Group TW was originated from Group MC and diverged at T1, Group JP was originated from Group MC (ancestral population) and diverged at T2; In Scenario 3, Group MC was originated from Group TW and diverged at T1, Group JP was originated from Group TW (ancestral population) and diverged at T2; In Scenario 4, Group TW was originated from Group MC and diverged at T1, Group MC and Group JP were originated from Group MC + JP (ancestral population) and diverged at T2; In Scenario 5, Group MC was originated from Group TW and diverged at T1, and Group TW and Group JP were originated from Group TW JP (ancestral population) and diverged at T2; In Scenario 6, Group MC and Group TW were originated from Group MC + TW (ancestral population) and diverged at T1, Group MC + TW and Group JP were originated from Group MC + TW + JP (ancestral population) and diverged at T2. **B**, Four demographic scenarios of changes in population size of *C. ramondioides*. NA and Na, ancestral population size; Ne, current population size; NB and Nb, population sizes between NA and Ne with NA < NB, NA > Ne, Nb < Ne, Na < Ne, t2 > t1. **C**, Prior and posterior distribution of parameters of best fit scenarios for demographic history of (a) Group MC, (b) Group TW, and (c) Group JP. **D**, Plots for fitness of competing and modeling checking for (a) Group MC, (b) Group TW, and (c) Group JP based on direct logistic regression, simulated in DIYABC.

Fig. S2. Maximum-likelihood phylogenetic tree obtained with by RAxML (Stamatakis, 2006), based on single nuclear polymorphism data of *Conandron ramondioides* individuals, with three outgroups of *Ridleyandra* sp. (see text). Numeric values indicate branch bootstrap support.

Fig. S3. Relationship between genetic and geographic distance for *Conandron ramondioides* based on single nuclear polymorphism data from 11 populations.

Fig. S4. Receiver operator characteristic curve tests the accuracy of Maxent model in (**A**) LIG, (**B**) LGM (CCSM4), (**C**) LGM (MIROC), (**D**) LGM (MPI-ESM-P), (**E**) PRESENT, and (**F**) FUTURE. AUC, area under the receiver operator characteristic curve; CCSM4, Community Climate System Model Version 4; LGM, Last Glacial Maximum; LIG, Last Interglacial period; MIROC, Model for Interdisciplinary Research on Climate; MPI-ESM-P, New Earth System Model of the Max Planck Institute for Meteorology.

Fig. S5. Jackknife test for the significance of bioclimatic variables performed by MaxEnt model in (**A**) LIG, (**B**) LGM (CCSM4), (**C**) LGM (MIROC), (**D**) LGM (MPI-ESM-P), (**E**) PRESENT, and (**F**) FUTURE. AUC, area under the receiver operator characteristic curve; CCSM4, Community Climate System Model Version 4; LGM, Last Glacial Maximum; LIG, Last Interglacial period; MIROC, Model for Interdisciplinary Research on Climate; MPI-ESM-P, New Earth System Model of the Max Planck Institute for Meteorology.